Structural Requirements for Proinflammatory Activity of Porin P2 Loop 7 from *Haemophilus influenzae*

Stefania Galdiero,[§] Mariateresa Vitiello,[‡] Pietro Amodeo,[||] Marina D'Isanto,[‡] Marco Cantisani,[§] Carlo Pedone,[§] and Massimiliano Galdiero*[,‡]

Department of Experimental Medicine, II University of Naples, Via De Crecchio 7, 80138 Naples, Italy, Department of Biological Sciences, Division of Biostructures, University of Naples "Federico II", and Istituto di Biostrutture e Bioimmagini−CNR, Via Mezzocannone 16, 80134 Naples, Italy, and Istituto di Chimica Biomolecolare−CNR, Sede di Pozzuoli, Via Campi Flegrei 34, Comprensorio Olivetti, Edificio 70, 80078 Pozzuoli, Naples, Italy

Received November 4, 2005; Revised Manuscript Received February 6, 2006

ABSTRACT: *Haemophilus influenzae* type *b* (Hib) is one of the leading causes of invasive bacterial infection in young children, characterized by inflammation mainly mediated by cytokines and chemokines. One of the most abundant components of the Hib outer membrane is the P2 porin, which has been shown to induce the release of several inflammatory cytokines. Synthetic peptides corresponding to loops L5, L6, and L7 activate JNK and p38 mitogen-activated protein kinase (MAPK) pathways, L7 being the most active peptide. Therefore, sequence−activity relationships and key residues were identified by elongating sequence to different extents, designing cyclic peptides, and performing an alanine scan of L7. The ability of mutant peptides to induce activation of signal transduction pathways and release of TNF-α and IL-6 has been determined, and, in conjunction with CD spectra, bioinformatics analysis, and molecular dynamics data, showed that 6 out of 8 amino acids contribute significantly to the overall activity. Molecular dynamics showed that L7 modifications increased loop rigidity and helicity after Gly6 mutation, thus, providing a possible structural explanation for observed loss of bioactivity. This work provides insights into essential molecular details of P2 that may impact on the pathogenesis of Hib infections where interruption of the signaling cascade could represent an attractive therapeutic strategy.

Haemophilus influenzae is a pathogenic Gram-negative bacterium responsible for a variety of infections in both children and adults, ranging from bronchitis to meningitis. *H. influenzae* is classified into two main groups: typeable (encapsulated) and nontypeable (nonencapsulated) strains. Six capsule serotypes have been described (a−f). Strong vaccination programs dramatically reduced the incidence of *H. influenzae* type *b* (Hib)[1] disease in the United States and Europe. However, significant health risks remain in developing countries and undervaccinated regions of western society. An understanding of structure−function relationships of Hib components may provide opportunities to develop novel antibacterial agents against diseases caused by Hib.

* Corresponding author. Phone: +39 081 5667646. Fax: +39 081 5667578. E-mail: massimiliano.galdiero@unina2.it.

[‡] Department of Experimental Medicine, II University of Naples.

[§] Department of Biological Sciences, Division of Biostructures, University of Naples "Federico II", and Istituto di Biostrutture e BioimmaginisCNR.

[||] Istituto di Chimica BiomolecolaresCNR.

[1] Abbreviations: CD, circular dichroism; DIEA, diisopropylethilamine; DMF, *N*,*N*-dimethylformamide; ECL, enhanced chemiluminescence; EM, energy minimization; Fmoc, fluorenylmethoxycarbonyl; Hib, *Haemophilus influenzae* type b; HOBT, 1-hydroxybenzotriazole hydrate; HPLC, high-pressure liquid chromatography; LDH, lactate dehydrogenase assay; MAPK, mitogen-activated protein kinase; MBHA, 4-(2′,4′-dimetoxyphenyl-Fmoc-aminomethyl)phenoxyacetamido-norleucyl-methoxybenzidrylamide resin; MD, molecular dynamics; OMP, outer membrane protein; PDB, protein database; PyBop, benzotriazol-1-yl-oxytripyrrolidinophosphonium hexafluorophosphate; SA, simulated annealing; TFA, trifluoroacetic acid; TFE, 2,2,2-trifluoro-ethanol.

Bacterial surfaces are important when considering the interaction with host cells and tissues in the context of pathogenesis and immunity to infections. However, to date, there have been no global studies aimed at the identification of the components of the outer membrane that are exposed on the bacteria surface; these studies may be critical in order to reduce the number of targets that can be used for the design of potential vaccines and may highlight domains that are likely to be directly involved in the interaction with the host (*1*). In particular, several bacterial components are involved in the modulation of pathogen−host cell interactions. The outer membrane of Gram-negative bacteria, embedded with diverse proteic and lipopolysaccharidic molecules, functions as a complex permeability barrier protecting the bacteria against harmful agents. Being a relevant component of the Gram-negative bacterial outer membrane, porins play an important role in pathogenesis of bacterial infections and stimulate immunological responses inducing the release of several cytokines (*2*−*4*).

Porin P2 of Hib (*5*), one of the best-characterized porins in terms of its functional characteristics, is the most abundant outer membrane protein (OMP) in nontypeable *H. influenzae* (NTHi) and in Hib; its molecular mass varies between 36 and 42 kDa, and it is present in all strains and functions as a porin (*6*). P2 contains 16 antiparallel β-strands crossing the outer membrane, eight large loops of variable length on the external surface of the bacterial membrane, and eight short periplasmic turns (*7*−*9*) (Figure 1).

10.1021/bi052262p CCC: $33.50
Published on Web 03/18/2006

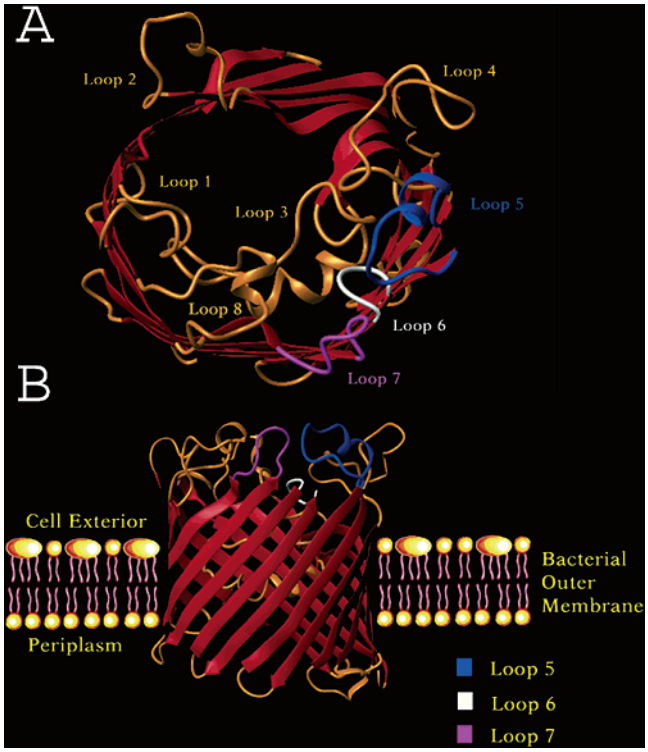

FIGURE 1: Three-dimensional model of the P2 monomer from Hib. (A) A slice horizontally through the barrel; loops L5, L6, and L7 are shown in different colors. (B) Overview of the molecule.

Sequence comparisons of P2 genes indicate that all transmembrane regions are relatively conserved among strains, while considerable heterogeneity exists in loop regions (*7*−*9*). This barrel spans the entire outer membrane, forming a trimer with the three-barrel axes almost mutually parallel and perpendicular to the membrane. As for other porins, one large loop (loop L3), folding back into the channel, determines effective pore cross section and consequent molecular exclusion limit, as well as its physiological and conductivity properties (*10*).

Recently, we demonstrated that porins from Hib induce activation of signaling pathways in U937 cells, and we also identified one of the phosphorylation pathways activated through the MEK1−MEK2/MAPK cascade (*8*). Peptide sequences corresponding to variable loop regions facing the cell exterior are able to activate such cascade; those exhibiting greatest diversity in both length and sequence are mainly involved in signaling pathways, and they provide a MAPK pathway activation similar to that of entire porin P2. In particular, surface-exposed loops L1, L2, L3, L4, and L8, involved in trimerization or in determination of pore size and functionality, are unable to significantly activate MEK1−MEK2/MAPK pathway, while loops L5, L6, and L7 showed prominent JNK and p38 activation, comparable to that induced by the whole protein.

In this study, we analyzed in detail the peptides corresponding to several analogues of the most active peptide L7 of Hib porin P2 in order to identify (a) relationships between porin structures and their interactions with host cells and (b) critical residues for MAPK cascade phosphorylation and for cytokine production. Specifically, we focused on TNF-α and IL-6 production (*11*, *12*) and their mRNA expression since these are the most-studied proinflammatory cytokines which induce many of the symptoms and signs that accompany the inflammatory disease and induce events such as septic shock (*13*).

Table 1: Amino Acid Sequences of Peptides

loop	sequence	protein fragment
L2	TKASENGSDNPGDITSK	69−85
L5	KYNESDEHKQQLNG	206−219
L6	SGYAKTKNYKIKHEK	239−253
L7	TSVDQGEK	280−287
β-strand 1	TNVELGGRLSIIAEQS	9−24
β-strand 3	FYAQGYLETR	57−66
scrambled	GVQKSDTE	280−287
Aspy	RKIRKENRMK	
AlaA	ASVDQGEK	280−287
AlaB	TAVDQGEK	280−287
AlaC	TSADQGEK	280−287
AlaD	TSVAQGEK	280−287
AlaE	TSVDAGEK	280−287
AlaF	TSVDQAEK	280−287
AlaG	TSVDQGAK	280−287
AlaH	TSVDQGEA	280−287
N1	RTSVDQGEK	279−287
N2	ERTSVDQGEK	278−287
CKR	KYERTSVDQGEKTR	276−289
CCC	CYERTSVDQGEKTC	276−289
C1	TSVDQGEKT	280−288

MATERIALS AND METHODS

Cell Lines. U937 monocytes (ATCC CRL-1593.2) were grown and differentiated as previously described (*14*). Cells were tested every 2 weeks by a PCR-based detection assay for micoplasma contamination (*15*).

Bacteria and Growth Conditions. *H. influenzae* type b (Hib), ATCC 9795 was grown in CY medium (*16*) for 18−24 h at 37°C; cells were harvested at the end of the exponential growth phase.

Preparation of the Porin. Porin was isolated and purified from bacterial cells as previously reported (*17*). The protein content of the porin preparation was determined by the method of Lowry et al. (*18*) and checked by SDS−PAGE according to Laemmli (*19*). All possible traces of LPS were revealed on SDS−PAGE stained with silver nitrate as described by Tsai and Frasch (*20*) and by the *Limulus*-amoebocyte-lysate assay (*Limulus* test) according to Yin et al. (*21*). When the *Limulus* test was used, LPS contamination in the porin preparation was estimated to be about 0.001% (w/w), compared with a standard Hib LPS solution. The pore-forming ability of our preparation was checked by a functional assay (liposome-swelling assay) after the incorporation into proteoliposome according to Nikaido and Rosenberg (*22*). Purity of the porin preparation from Hib and analysis of N-terminal sequence (AVVYNNEGTNV) of the isolated protein were reported in a previous paper (*17*).

Peptides Synthesis. Peptides corresponding to loop regions were prepared by standard 9-fluorenylmethoxycarbonyl polyamine solid-phase syntheses, using a PSSM8 multispecific peptide synthesizer (Shimadzu Corporation Biotechnology Instruments Department, Kyoto, Japan). The syntheses, purification, and characterization of these peptides have been described previously (*8*). Amino acid sequences of all synthesized peptides are reported in Table 1. The P2 porin sequences from 11 strains were obtained from the Swiss-Prot database.

Cell Stimulation and Preparation of Cell Lysates. U937 cells (3×10^6 cells/mL) were stimulated with different

Table 2: Protein Loops in PDB Entries Structurally Aligned to L7 Peptide

protein/fold family	protein region	loop sequence	PDB code
	Gly-I		
extracellular Asp protein *Candida tropicalis*	T117−G122	TSVDQG	1J71
secreted Asp protease *C. albicans*	T117−G122	TSIDQG	1EAG
S. pneumoniae H lyase	V384−E388	VDQGE	1EGU
Isocitr. dehydrog. F *B. subtilis*	Q3−K6	QGEK	1HQS
CapCRP	Q32−K35	QGEK	1HW5
neurofibrinomin	D1217−E1220	DQGE	1NF1
	Gly-II		
L-alanine dehydrogenase	V268−G271	VDQG	1PJC
barley grain peroxidase 1	D293−E296	DQGE	1BGP
catalase Hpii *E. coli*	D712−E715	DQGE	1GGE
thymidine kinase from *Herpes virus 1*	D108−E111	DQGE	1E2H
	no-Gly		
methane monooxygenase Hydroxylase	T24−Q28	TSVDQ	1MHY
triosephosphase	S79−Q82	SVDQ	3YPI
Streptococcal pyrogenic exotoxin A1	S37−Q40	SVDQ	1B1Z
ferrodoxin	S55−Q58	SVDQ	1DOX
human dihydroorotate dehydrogenase	T187−E193	TSVDAAE	1D3G

concentrations of stimuli for different time periods in 96-well polypropylene plates. After incubation, the cells were prepared as previously reported (*8*) and used for enhanced chemiluminescence (ECL) Western blot analysis.

Analysis of Kinase Phosphorylation by Western Blotting. Cell lysates were immunoprecipitated and used for Western blotting following standard procedures as previously reported (*8*).

Cytokine Release. All assays were carried out using U937 cells (3×10^6 cells/mL) stimulated with different concentrations of stimuli for 24 h at 37 °C in 5% CO_2. After incubation, samples were centrifuged at 1800 rpm at 4 °C for 10 min, and the supernatants were collected and stored at −70 °C. IL-6 and TNF-α protein concentrations were measured with enzyme-linked immunoadsorbent assay (ELISA) kits from Roche (Roche Diagnostics, Germany). Assays were performed as described in the manufacturer's instructions.

Cytokine mRNA Analyses. All assays were carried out using 1×10^6 U937 cells/mL cultured in RPMI 1640 without FCS for 24 h at 37 °C. The stimuli were added to suspensions of U937 cells in complete medium for 4 h, the time having been determined in preliminary experiments as that giving optimal cytokine expression. After incubation, cells were collected and washed, and total RNA was extracted by High Pure RNA Isolation kit (Roche Diagnostics SpA, Milano, Italy). Reverse transcription (RT)-PCR was performed to determine relative quantities of mRNA for IL-6 and TNF-α as previously described (*14*) by using specific primers.

Inhibitors of Signal Transduction. In some experiments, before stimulation, U937 cells (3×10^6 cells/mL) were pretreated with different inhibitors: 4-(4-fluorophenyl)-5-(4-pyridyl)1*H*-imidazole (SB-203580) (Calbiochem-Novabiochem GmbH, Schwalbach, Germany) (10 μM for 1 h), a specific inhibitor of the p38 pathway and of another cytokine receptor kinase such as TGF-β type I receptor; JNKinhibitor-1 (JNK inhibitor) (L-JNKI1) (Alexis Biochemicals, San Diego, CA) (1 μM for 1h), a peptide that specifically binds and inhibits JNK activity (*23*−*25*).

Circular Dichroism Measurements. Spectra were recorded using a Jasco J-715 spectropolarimeter in a 1.0 cm quartz cell at room temperature. Solutions of peptides (0.2 μM) were prepared in water and in 80% TFE. Each spectrum was averaged on three consecutive scans from 260 to 195 nm, with a bandwidth of 3 nm, a time constant of 16 s, and a scan rate of 10 nm min^{-1}. Helicities were calculated from measurements of their ellipticity at 222 nm (*26*).

Molecular Dynamics and Structural Alignments. Molecular dynamics (MD), simulated annealing (SA), and energy minimization (EM) calculations were run with AMBER 6 (*27*). AMBER 6 and MOLMOL (*28*) were used for structural analysis. Homologous loop sequences were obtained with BLAST 2.2.9 (*29*).

Calculations were performed with the Sander module of AMBER6 (*27*), with AMBER all-atom 1994 parametrization (*30*). Conformational sampling was obtained by SA as previously described (*31*), with no experimentally derived restraints. The best 50 structures in terms of total energy were clusterized and analyzed. Regular extended ($\varphi = -150°$, $\psi = 150°$) and helical ($\varphi = -57°$, $\psi = -47°$) conformations of each peptide were generated and energy-minimized with the same protocol.

The extended and helical EM structures of L7 and AlaF peptides, after electrostatic neutralization with a Na^+ ion, were solvated with the LEaP module of AMBER 6.0 package (*27*, *30*), in rectangular boxes of TIP3 water molecules (*32*) with an isotropic clearance of 10 Å and a "closeness" parameter value of 1.0 for L7 in the extended conformation and consequently adjusted values of these parameters for L7/helix, AlaF/extended, and AlaF/helix, to obtain the same number of water molecules (1477) in each system. After constrained equilibration (1000 steps of EM, 120 ps constant volume/temperature (nVT) MD, and 80 ps of constant pressure/temperature (nPT) MD, a 2 ns unrestrained/unconstrained nPT MD was run, collecting coordinates, velocities, and energies every 500 steps in the last 1 ns for analysis. MD parameters are listed in ref *33*.

First, proteins containing at least four adjacent residues from the L7 sequence were selected in the PDB database (*34*) (Table 2). The overlapping sequences were aligned, and the corresponding backbone atoms underwent best fit superposition by fitting each segment to either the "best overall template" (PDB code 1J71), that is, the structure sharing the highest similarity with L7, corresponding to

residues 1−6, or to the "best C-terminal template" (PDB code 1EGU), sharing only five residues (3−7) with L7 but including the Glu7 residue, to include at least four residues in each fit. For those structures containing the last four L7 residues whose overlap with 1EGU only amounts to three residues, inclusion of one more N-terminal residue provided the fourth fitted position.

Lactate Dehydrogenase (*LDH*) *Assay*. LDH assay was carried out according to manufacturer's instructions using a cytotoxicity detection kit (Roche Diagnostic SpA, Milano, Italy).

Reproducibility. Gels were scanned for densitometry analysis by Sigma Gel software averaging the results of three different experiments.

RESULTS

Peptide Design. Sequences of loops L5, L6, and L7 were chosen according to a theoretical model as previously reported (*8*). Following the results of cytokine release assay, three new peptides derived from loop L7 were designed and synthesized with (1) an extra C-terminal Thr residue (C1); (2) an extra N-terminal Arg residue (N1); (3) two extra N-terminal Glu−Arg residues (N2).

After comparison of activation of the signal transduction pathways, original L7 loop, the most active among all synthesized peptides, underwent an Ala-scanning mutagenesis study. Alanine was selected as the replacement residue because of its lack of charge and of bulky or functional side groups.

Two other peptides containing some extra residues from β-strands preceding and following loop L7 in the P2 sequence were synthesized: CKR, corresponding to the sequence KYER-loop7-TR, to evaluate effects of mere elongation at both ends, and CCC (CYER-loop7-TC), obtained from the former after replacement of the first and the last residue with Cys and subsequent cyclization, to verify if this constraint induced a correct conformation for L7 loop.

Control peptides were synthesized and tested to verify the reliability of our experiments and that cytokine release was only inducted by active sequences. In particular, we tested (i) two peptides corresponding to β-strands β1 (Thr9−Ser24) and β3 (Phe57−Arg66) of P2 porin, to verify that conserved regions located in membrane interior were not able to induce TNF-α and IL-6 releases; (ii) a highly hydrophilic undecapeptide, ASPY, to demonstrate that even a highly hydrophilic sequence was unable to induce any response; (iii) a scrambled peptide, with same composition but different sequence from L7, to state sequence-dependency of the results; and (iv) a peptide corresponding to loop L2, to verify that peptides unable to induce MAPK cascade activation were also unable to induce TNF-α and IL-6 release. In any case, no significant cytokine release was induced by control peptides.

MAPK Pathway Signaling Activation by L7 Analogues. Having previously demonstrated (*8*) that L7 was the most active among the peptides corresponding to external loops of P2 porin at inducing MEK1−MEK2/MAPK pathways (in particular of JNK and p38) (Figure 2A), we now compared activating phosphorylation capabilities of synthesized peptides by individual tests on U937 cells.

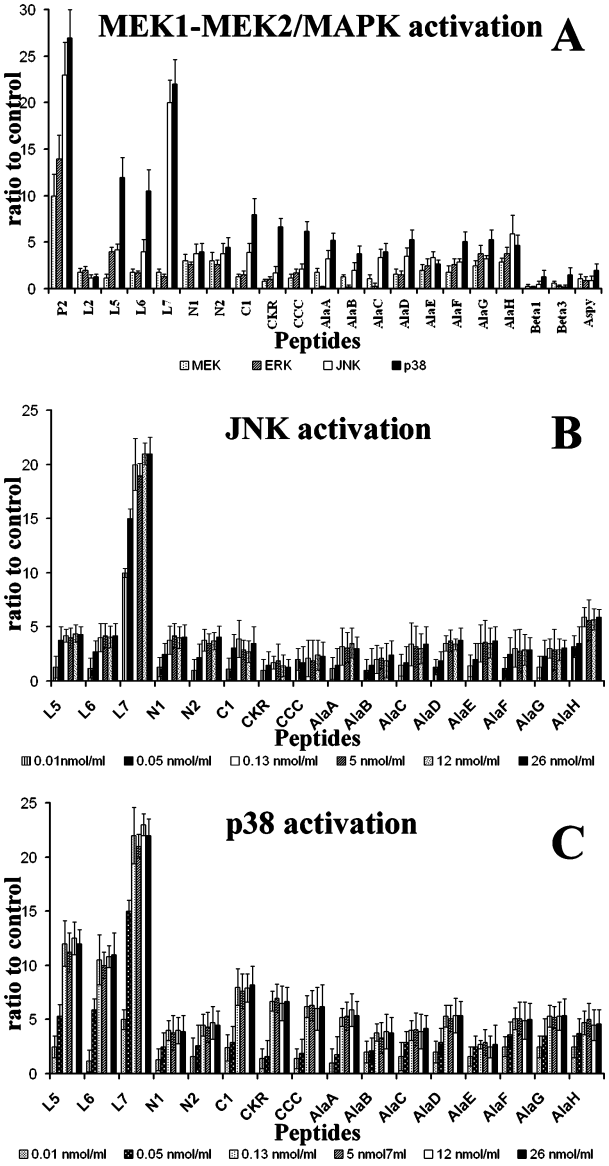

FIGURE 2: (A) MEK1−MEK-2/MAPK activation in U937 cells in response to a dose of 0.13 nmol/mL and at a stimulation time of 10 min. (B) JNK activation and (C) p38 activation at various doses of active peptides after 10 min of stimulation.

Peptide concentrations of 0.01, 0.05, 0.13, 5.0, 12, and 26 nmol/mL were assayed (Figure 2B,C; inactive peptides not shown). As for the entire protein, signals from active peptides were visible 3 min after treatments, with a phosphorylation peak at 10 min, persisting for at least 20 min thereafter and going back to standard levels by 60 min (data not shown). A standard concentration of 0.13 nmol/mL and stimulation times of 10 min were chosen for subsequent experiments.

Induction of signal transduction pathways by C1, N1, N2, CKR, and CCC was assayed. Decapeptide N2 (protein fragment Glu278−Lys287) and nonapeptides N1 (Glu278−Lys287) and C1 (Thr280-Thr288) strongly induced an increase in immunoreactive bands of JNK and p38, while activated less efficiently the phosphorylation of MEK1/2 and ERK1/2. The 14 aa peptides CKR and CCC induced a significant activation of p38 but not of MEK1/2, ERK1/2, and JNK. The eight L7 Ala-scanning peptides AlaA−AlaH (Thr280−Lys287) all induced a significant increase in

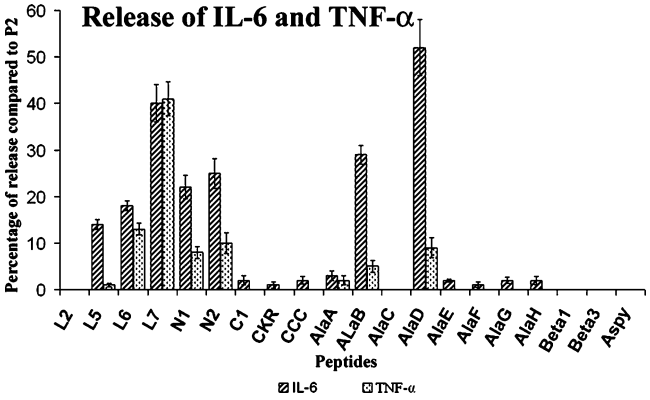

FIGURE 3: IL-6 and TNF-α release after peptide treatment. The results shown are the average of three independent experiments, and the error bars indicate the standard errors of the means.

phosphorylation, while all control peptides exhibited no activation of the MEK1−MEK2/MAPK pathways as well (Figure 2B,C).

Release of IL-6 and TNF-α by L5, L6, L7, and L7 Analogues in U937 Cells. Peptides L7 and L2, at a concentration of 130 nmol/mL, induced IL-6 and TNF-α cytokine responses, amounting to approximately 40% and 20%, respectively, of that produced by the entire P2 protein. Loop L5 was still able to induce release of IL-6 (approximately 15%), while only traces of TNF-α were detected (Figure 3).

We subsequently assayed longer homologues and Ala-scanning mutants of L7. Table 1 summarizes the sequences of all examined peptides; relative efficiencies of all peptides to stimulate IL-6 and TNF-α release are shown in Figure 3. Only responses to a 130 nmol/mL peptide concentration, which gave the highest increases in both cytokines release for all peptides, are presented in Figure 3.

Peptides L2, C1, CKR, CCC, AlaA, AlaC, AlaE, AlaF, AlaG, and AlaH did not induce a significant release of IL-6 and TNF-α (Figure 3). Peptides AlaB and AlaD were able to induce both TNF-α and IL-6 cytokine responses. In particular, both peptides induced a minor release of TNF-α and a much higher release of IL-6. AlaD was able to induce a release of IL-6 comparable to L7. Peptides N1 and N2 gave a high yield in IL-6 and a smaller release of TNF-α.

The induction of cytokine release was dose-dependent. L5, L6, N1, and N2 only induced a small release of IL-6 at a concentration of 0.13 nmol/mL, when L7 already produced approximately 15% of IL-6 release due to P2. Peptide concentrations of 13 nmol/mL induced the maximum amount of IL-6 for all peptides, higher concentrations providing no further increase in activity. AlaB and AlaD, instead, were able to induce the maximum release of IL-6 only at concentrations higher than 130 nmol/mL (Figure 4A).

Peptide concentrations as low as 0.13 and 1.3 nmol/mL were not sufficient to release detectable amounts of TNF-α, and the optimal concentration was detected at 130 nmol/mL (Figure 4B).

These peptide concentrations were not toxic for cells, and the treatment not induce any significant release of LDH in cell supernatants. No significant cytokine release was induced by any control peptides.

IL-6 and TNF-α mRNA Expression by L5, L6, L7, and L7 Analogues in U937 Cells. An analysis of IL-6 and TNF-α mRNA in U937 cells treated for 4 h with L5, L6, L7, and Ala-peptides was performed using RT-PCR. U937 cells were stimulated with optimal peptide concentrations for release of IL-6 and TNF-α. All experiments were performed in triplicate and gave similar results.

As detected by RT-PCR analysis, cytokine mRNA bands were present for IL-6 and TNF-α after treatment with P2, L5, L6, L7, N1, N2, AlaB, and AlaD. The results obtained were confirmed by quantization of mRNA using Sigma Gel software. As a control, we measured the levels of β-actin mRNA, which is a cell cycle-independent mRNA. Actin mRNA levels remained unchanged, indicating that observed changes in cytokine mRNA levels were not caused by a general increase in all poly(A)$^+$ RNA species (Figure 5).

Involvement of MAPK Pathways in TNF-α and IL-6 Release by L5, L6, L7, and L7 Analogues. Porin P2 peptides corresponding to loop-variable regions stimulate the MEK1−MEK2/MAPK cascade; in particular, surface-exposed loops L5, L6, and L7 showed prominent JNK and p38 activation, comparable to that induced by the entire protein. To confirm the role of JNK and p38 pathways in the induction of IL-6 and TNF-α by active sequences, the effects of specific inhibitors were examined (Figure 4C,D).

To identify the role of JNK activation in peptides TNF-α- and IL-6-induced up-regulation, we tested the effects of L-JNKI1, which specifically inhibits phosphorylation of downstream kinases by JNK. Pretreatment of U937 cells with L-JNKI1 (1 μM) strongly decreased IL-6 and TNF-α release after peptide stimulations, indicating that the JNK pathway is required for IL-6 and TNF-α production (Figure 4C,D).

The p38 inhibitor SB203580 (10 μM) bicyclic imidazole compound, specifically inhibiting phosphorylation of downstream kinases by p38 isoforms a and b and another cytokine receptor such as TGF-β type I receptor, significantly reduced cytokines release in response to analyzed peptides, indicating that p38 is one of the MAPK pathways required for IL-6 and TNF-α activation (Figure 4C,D). The concentrations of inhibitors and porins or LPS used were not toxic for cells, and treatment did not induce any significant release of LDH in cell supernatants.

Secondary Structure of Synthetic Peptides. Secondary structure preferences of our peptides were evaluated by CD spectroscopy. All peptides had a strong negative band around 200 nm, typical of an unordered structure in aqueous solution. Peptides were then studied in TFE/water mixtures (80% TFE) to evaluate their intrinsic helical propensity. All peptides presented a very low helical propensity, with the partial exception of C1, CCC, and AlaF, which exhibited some (between 15 and 20%) α-helical character. In particular, all peptides, as expected, showed largely random coil spectra in water, and those exhibiting some α-helical content also provided the lowest cytokine release inducing activities. So, occurrence of α-helical structure appears to diminish or abolish activity, and peptide flexibility is possibly a major prerequisite for activity.

Molecular Dynamics Simulations and Structural Alignment Analyses. From activity data, L7 appeared to best mimic the behavior of intact P2; thus, it was selected as the template sequence for sequence−activity or structure−activity relationship studies (and its numbering was used throughout the discussion).

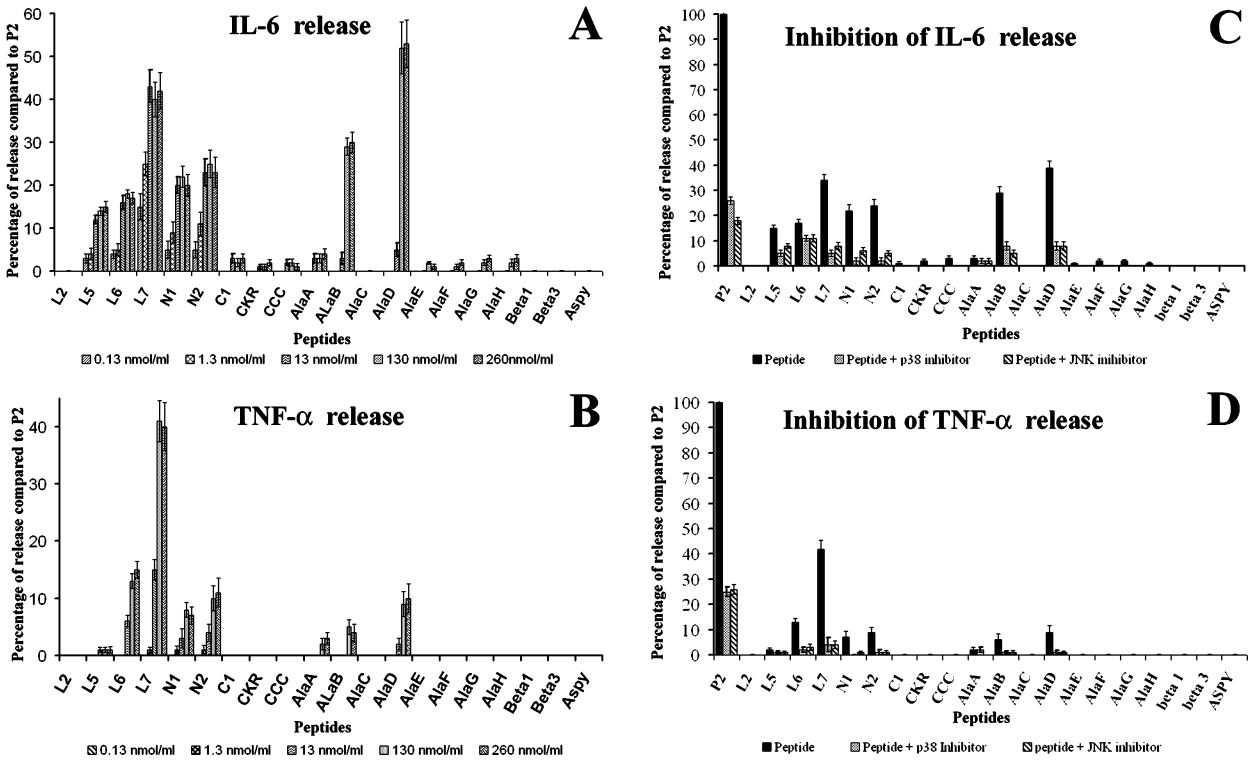

FIGURE 4: Concentration response of active peptides on IL-6 (A) and TNF-α (B) production. Analysis of the effects of the SB203580 (p38 inhibitor) or L-JNKI1 (JNK inhibitor) on IL-6 (C) and TNF-α (D) release induced by peptides stimulation. The results shown are the average of three independent experiments, and the error bars indicate the standard errors of the means.

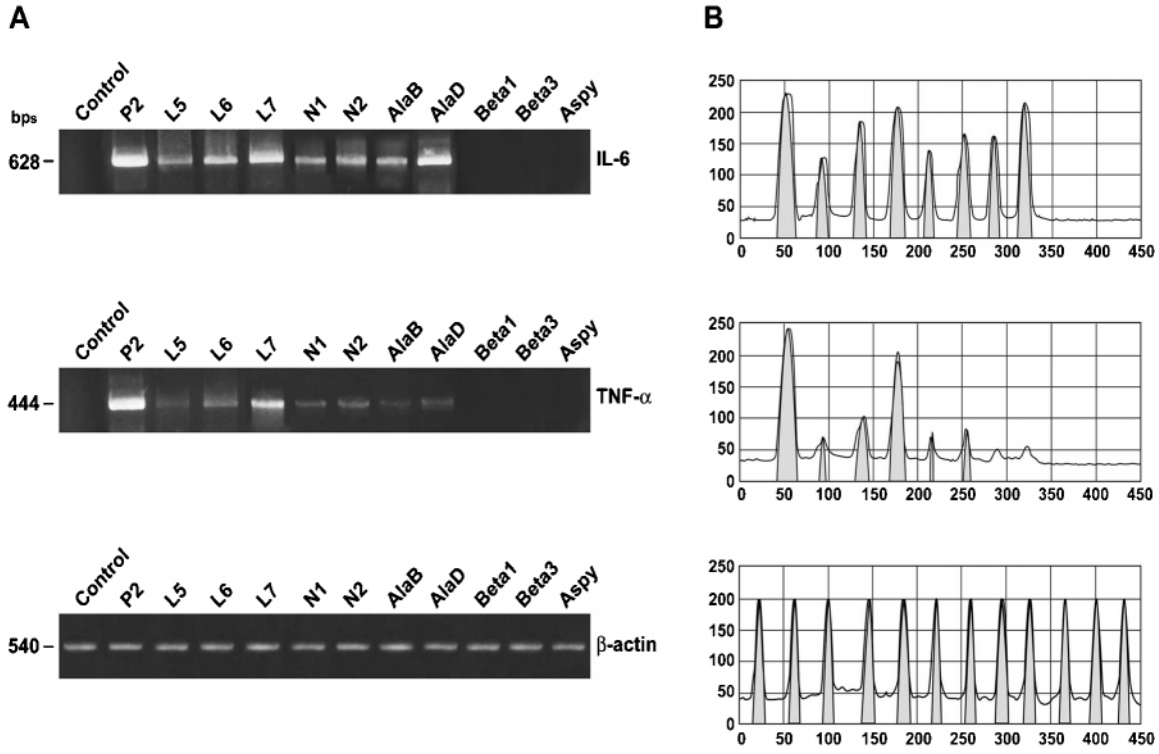

FIGURE 5: IL-6 and TNF-α mRNA expression in U937 cells 4 h after stimulation (A) U937 cells (1×10^6/mL), resuspended in RPMI 1640, were stimulated with peptides (130 nmol/mL) and then subjected to RNA extraction and RT-PCR amplification. Reaction products were run on a 1.5% agarose gel in the presence of appropriate molecular mass markers; β-actin was the positive transcription control. (B) RT-PCR quantitation of cytokine results was analyzed by Sigma-Gel software.

Gly6 was soon identified as a critical residue for the conformational behavior of L7, and its substitution with Ala led to the totally inactive AlaF, which exhibited some helical structure in TFE/water and less unfavorable relative stabilities of helical versus extended conformations than L7 in 2 ns MD simulations in water. In particular, helical turns in AlaF occurred in 0% and 29% of the sampled structures for simulations started from extended and helical conformations, respectively, while 0% and 4.5% of helices were observed in corresponding simulations for L7. C-terminal elongation

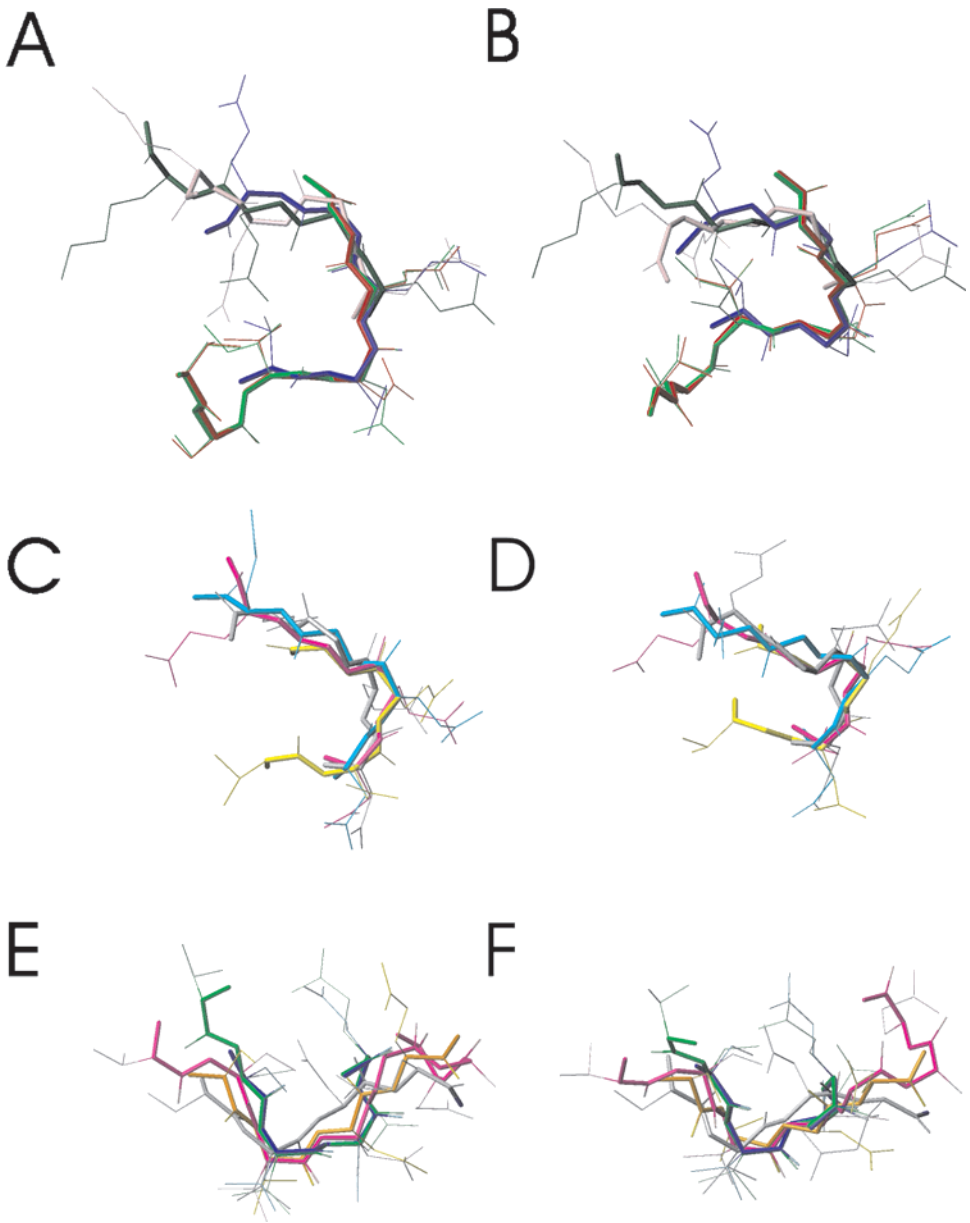

FIGURE 6: Structural alignment of protein loops homologous to L7 peptide. Gly-I, Gly-II, and no-Gly loop fold families are shown separately in panels A−B, C−D, and E−F, respectively. 1NF1, the worst fitting sequence in the Gly-I bundle, is omitted for clarity. The right view is obtained from the left one by a 45° rotation about the horizontal axis of the figure. Only backbone (thick sticks) and side chain heavy-atom (thin sticks) bonds are shown. PDB codes/colors are for Gly-I structures (A, B) 1J71/red, 1EAG/green, 1EGU/blue, 1HQS/dark green, 1HW5/pink; for Gly-II (C, D) 1PJC/yellow, 1BGP/cyan, 1GGE/magenta, 1E2H/gray; for no-Gly (E, F) 1MHY/green, 3YPI/blue, 1D3G/magenta, 1B1Z/orange, 1DOX/gray.

of L7 also appeared to favor helicity, as shown by CD data in TFE/water for CCC and C1 analogues.

These data, together with biological results, stressed the correlation between helix propensity and loss of activity, suggesting relevant roles for peptide terminal groups and overall peptide flexibility. In this view, a complementary approach to the CD−MD study was attempted, based on a compared analysis of well-defined three-dimensional structures of proteins in the PDB database (*34*) containing segments highly homologous to L7.

Inspection of secondary structure patterns in the structural alignment evidenced a strong segment clustering in two distinct families of secondary/tertiary structures. Whenever a Gly occupied the 6th position in L7 sequence, a loop systematically occurred, with Asp−Gln (and, often, adjacent residues) in a "bend" conformation, with the only partial exception of 1BGP, whose loop includes a single Ser-Asp-Gln 3_{10} helix turn. L7 homologous sequences exhibited short loops (eight residues), either joining two β-strands or two α-helices, in all 11 proteins where Gly6 was present. In the absence of Gly6, instead, sequences either formed large loops (or even unstructured terminal regions) or were partly (totally in -Val-Asp-Gln-Ala-Glu-Lys- fragment of 1F1F and 1KIB) α-helical.

Superposition of the aligned segments showed that Gly-containing sequences clustered in space and, despite their loop-propensity, defined a common "envelope" and preserved orientation of the central L7 side chains, even when "patchworks" of overlapping motifs spanning the whole L7 sequence were considered (Figure 6). In particular, the 11 structures clustered in two slightly different conformational families. In the first set (Gly-I), formed by six structures

(1J71, 1EAG, 1EGU, 1NF1, 1HQS, 1HW5, Figure 6A,B), the whole L7 sequence was covered by the bundle, with at least two overlapping sequences for each position. Secondary structure analysis identified three sequential or partly overlapped β-turns, except for short (i.e., including less than five conserved L7 residues) or protein terminal sequences, where only one or two canonical turns may be detected. According to the Hutchinson−Thornton classification (*35*), subtypes of β^{VI}-turn occurred in all sequences except 1NF1, and β^{VIII} was detected in 3 out of the 6 sequences. The overall segment envelope formed a wide "U-shaped" loop, with Asp and Gly at the corner positions, Gln at the bottom of the "U", and the two arms running almost parallel. The distance between N-terminal amino and C-terminal carboxyl groups ranged from 5 to 6 Å; this was too much for a direct salt-bridge interaction but fully compatible with a fluctuating electrostatic stabilization of L7 fold. However, arm end arrangements were affected by a larger variability than the rest of the loop, because (a) they were contributed by just two templates at each end; (b) Thr−Ser sequence was provided by very homologous proteins (1J71 and 1EAG); (c) one of the two C-terminal templates, 1HQS, contributed with its N-terminus; and (d) they were more influenced by the rest of the proteins than the central loop region, typically more external and independent from interaction with protein core. As also suggested by L7 conformational analysis, electrostatic interactions between ends can further stabilize L7 conformations similar to those detected in this first set.

The second family (Gly-II), including four structures (1PJC, 1BGP, 1GGE, 1E2H), featured a narrower loop with just two residues (Asp−Gln) forming the bottom of the "U" (Figure 6C,D), two sequential or partly overlapped β-turns, systematic occurrence of β^{VIII}, and absence of β^{VI}. Unfortunately, Gly-II members only spanned 5 out of the 8 L7 positions, lacking the first two and the last residue in the sequence, thus, providing no useful information on "U" arms and on interactions between sequence ends, although the narrower "U" structure suggested the occurrence of stronger interaction in Gly-II than in Gly-I

A similar analysis of sequences lacking Gly6 (no-Gly, Figure 6E,F) easily showed their higher conformational dispersion, and their only common trend, in fact, was a "negative" one, that is, the lack of any correlation between sequence ends, with just a subset of the structures exhibiting some helical propensity.

DISCUSSION

It is becoming increasingly clear that the virulence of any particular microrganism is the result of complex interactions between the organism and its host. Signals leading to cellular activation are often generated at the cell surface after binding of receptors to their appropriate ligands. This study is the first to identify those amino acid sequences of porins that are likely to be involved in cytokine synthesis.

Data from literature indicate that peptide sequences corresponding to superficial loops are responsible for most of the biological activity of porins. Surface-exposed loops present great sequence variability compared to transmembrane β-strands. Thus, it is particularly interesting to identify key structures in the amino acid sequences of surface-exposed loops to be used as templates in the design of new therapeutic agents against a broad range of Gram-negative bacteria. We have examined the effects of synthetic peptides corresponding to loops of Hib P2 on MAPK signaling cascades activation and cytokine synthesis. A model of the protein P2 (Figure 1) enabled us to better understand the role played by each loop (*8*). Loops L1, L2, and L4 are important for monomer−monomer interactions within the porin trimer; loop L3 is internal; loops L5, L6, and L7 are superficial; loop L8 contributes to form the channel opening on the external side. Surface peptides corresponding to loops L5, L6, and L7, which in the model do not seem to have any obvious structural function, have prominent JNK and p38 phosphorylation induction, comparable to that induced by the entire protein (*8*). Our results demonstrate that stimulation of U937 cells by L5, L6, and L7 induces IL-6 and TNF-α production and that this production is also mediated by MAP kinase phosphorylation. Interestingly, inhibition of kinase phosphorylation correlates with partial inhibition of cytokine production. In fact, using highly specific inhibitors of JNK and p38 activation, we were able to verify the requirements of JNK and p38 pathways for cytokine synthesis by L5, L6, and L7, this latter exhibiting the highest biological activity within the set. Responses induced by L5 and L6 were qualitatively similar to, but quantitatively weaker than, L7.

In this study, sequence−activity relationships were explored both by a point-mutation approach, based on Ala-scanning of the whole L7 sequence, and by elongating L7 sequence to different extents either at the N-terminus only (N1 and N2), at the C-terminus only (C1), or at both termini (CKR). In addition, a cyclic form, closed by a disulfide bridge between two Cys residues introduced at the ends of an elongated L7 sequence, was also tested (CCC).

Addition of one residue at L7 C-terminus yielded a peptide with no measurable release of IL-6 and TNF-α, although it is still able to induce activation of MAPK kinases. Addition of one or two residues at the N-terminus interestingly resulted in two peptides that were still able to induce release of IL-6, while only traces of TNF-α were detected. Addition of residues at both L7 termini determined an almost complete drop in activity. These results clearly show that the octapeptide L7 is the most active derivative among loops of protein P2.

Cyclization by introduction of a disulfide bridge was tested to determine if generically constraining the two L7 termini on the same side of the loop and/or decreasing its mobility could improve observed biological properties. Both CKR and CCC analogues were completely inactive, possibly suggesting that accessible conformations to these peptides differed significantly from those occurring in the intact P2 protein, and that biological activity may rely on strict conformational requirements for L7 loop.

While all peptides discussed above provided data mostly related to the overall conformational properties of P2 L7 loop, local information about relative contributions of each of the eight L7 amino acid side chains was obtained by an Ala-scanning mutagenesis study. Mutants were synthesized, and their ability to induce activation of signal transduction pathways and release of IL-6 and TNF-α, mRNA IL-6 and mRNA TNF-α transcripts were determined. Ala-scanning indicated that six out of eight side chains contribute significantly to the overall activity, and only two residues,

serine (AlaB) and aspartic acid (AlaD), are replaceable with no appreciable loss (or, even, with an increase) of observed activity. As the conformation-inducing properties of Ser and Asp do not differ appreciably from that of Ala, it is quite reasonable to hypothesize that side chains of these two residues in L7 are not involved in important interaction for biological activity.

Structure−activity relationships and, in particular, conformational preferences of L7 and its analogues were studied by a combination of CD spectra, molecular mechanics (simulated annealing (SA)-molecular dynamics (MD) approach), and 3D-structure comparative analysis of protein segments highly homologous to L7, occurring in structurally determined proteins.

The most striking result provided by activity values of L7 analogues is the high sensitivity of peptide activity toward the slightest changes in sequence. Both CD data and conformational analysis in solution indicate that L7 in water is a flexible peptide. These results may suggest the hypothesis of a strong influence of the nature of each residue in L7 sequence over its activity, with a limited importance of its conformational preference. However, the dramatic reduction, up to total loss, of activity upon mere peptide elongation, with retention of the L7 sequence, somewhat contradicts this hypothesis, suggesting either a relevant role of L7 intrinsic conformational properties or an accidental involvement of L7 terminal amino and/or carboxyl groups, or both, in activation processes.

CD and molecular dynamics studies on the alanine derivatives showed that the presence/absence of the Gly6 residue appears to act as the unique switch determining the observed local folding. Moreover, a comparison of these results with activity data shows that an increased propensity for helix formation is systematically associated with total loss of activity. However, both studies neither assessed the eventual role of charged L7 terminal group nor led to positive information on the three-dimensional structure of L7 and its analogues in water, because of the high overall flexibility of the peptides.

Structural alignment of protein fragments highly homologous to L7 showed that, whenever a glycine is present in position 6 of the L7 sequence, L7 homologues belong to short loops (8 residues) between two β-strands or two α-helices. In the absence of Gly6, the sequences form larger loops or even α-helices. Gly-containing sequences cluster into two slightly different main conformational families, Gly-I and Gly-II. In Gly-I, three sequential or partly overlapped β-turns occur. The two arms of the "U-shaped" loop run almost mutually parallel, at a distance compatible with fluctuating electrostatic fold stabilization, and the end arrangement of the two arms are, however, potentially more affected than the rest of the loop by specific interactions with template protein cores. Gly-II structures contain a narrower loop, and just two residues (Asp−Gln) form the bottom of the "U" and two sequential or partly overlapped β-turns. When sequences lacking Gly6 are analyzed, the most evident results are their higher conformational dispersion and their greater tendency to helix formation.

The sequences of *Haemophilus* P2 porins from 10 different strains were aligned, and the sequences of loop 7 from different strains are reported in Table 3. The results of the alignment of L7 sequences from different strains of P2 protein correlate well with our findings relative to the importance of the most conserved glycine residue and to the ensemble of experimental data here presented. Thus, our findings provide a possible explanation at atomic level of the observed sensitivity of functional properties of L7-derived peptides to even minor changes in peptide length and composition, in terms of a partial to total inactivation of a loop-derived molecule after reduction of its flexibility and/or alteration of its intrinsic conformational preferences. Similarly, other proteins homologous to P2 (*Candida albicans* secreted aspartyl proteinase, *Bacillus subtilis* isocitrate dehydrogenase, and *Streptococcus pneumonia* hyaluronate lyase) (*36*−*38*) contain loops that exhibit reduced affinity for their substrates after a decrease in their flexibility. Perhaps it is this lack of rigidity that enables these loops regions to move and expose themselves to the interaction with other molecules, but also the specific fold of the loop seems to play an important role in determining biological activity of P2 and its derivatives. However, presently available experimental and computational data only allow to say that a structural prerequisite of peptide activity is low helical propensity, possibly associated to formation of U-turn structures, as those exhibited by other (non-porin) peptides homologous to L7.

Table 3: Amino Acid Sequences of Loop 7 from Different Strains of Protein P2

strain	peptide sequence
P2	T-SVDQGEK
P46025	T-SVNQGKN
Q48220	N-SVDQGKK
P43839	T-SVDQGEK
P46026	T-SVNQGKN
P46027	T-SSDEGKK
Q48216	N-SVDQGKK
Q48217	N-SVDQGKK
Q48218	D-SVDQGKK
Q48219	N-SVDQGKK
Q48221	INSVDQGEK

Our data also seem to correlate with recently published atomic force microscopy studies on porin OmpF from *Escherichia coli*, analyzing the voltage- and pH-dependent conformational changes of extracellular loops (*39*). They suggest that the observed conformational changes, which are accomplished by the closure of the channel entrance, may represent a mechanism that the cells have evolved to protect themselves from drastic changes of the environment (*39*). Thus, the conformational flexibility of extracellular loops and their variability in length and amino acid sequence may be a fundamental characteristic of domains that are directly involved in the interactions with complementary structures of the host.

L7 loop sequence can be included among the microbial structures that initiate innate immune responses. Cellular responses are a result of coordinated outputs of activation against specific sequences, among which L7 is conserved in proteins from eukaryotic cells and also other microorganisms, thus, indicating a common evolutionary pattern. Extensive flexibility of this region may provide an explanation to different signal pathways involved at a qualitative and quantitative level. Moreover sequence conservation can justify the weak or absent adaptive immune response, eventually shown by some hosts. Surface amino acid

sequence variability among OMP antigens is probably responsible for poor efficacy of vaccines including nonspecific OMPs (*40*). On the contrary, the identification of active domains in porins suggests that it may be possible to generate specific inhibitors. Recently, atomic force microscopy offers new opportunities to probe functionally related conformational changes in surface membrane proteins directly in an aqueous solution which together with activity studies may provide information on the relative exposure of domains in outer membrane proteins of critical importance when selecting sequences to use as potential vaccines (*1*).

Thus, the structure of L7 is a good target for analysis with constrained peptides and for the design of complementary molecules. These results are opening up new strategies also for therapy of septic shock and are providing signposts for possible mechanisms of action of other bacterial porins in controlling cytokine network interactions.

ACKNOWLEDGMENT

This work was supported by funds from Regione Campania LR52002 Project No.107.

REFERENCES

1. Dufrene, Y. F. (2004) Using nanotechniques to explore microbial surfaces, *Nat. Rev. Microbiol. 2*, 451−460.
2. Achouak, W., Heulin, T., and Pages, J. M. (2001) Multiple facets of bacterial porins, *FEMS Microbiol. Lett. 199*,1−7.
3. Galdiero, M., Cipollaro de l'Ero, G., Donnarumma, G., Marcatili, A., and Galdiero, F. (1995) Interleukin-1 and interleukin-6 gene expression in human monocytes stimulated with *Salmonella typhimurium* porins, *Immunology 86*, 612−619.
4. Galdiero, M., De Martino, L., Marcatili, A., Nuzzo, I., Vitiello, M., and Cipollaro de l'Ero, G. (1998) Th1 and Th2 cell involvement in immune response to *Salmonella typhimurium* porins, *Immunology 94*, 5−13.
5. Yi, K., and Murphy, T. F. (1997) Importance of an immunodominant surface-exposed loop on outer membrane protein P2 of nontypeable *Haemophilus influenzae*, *Infect. Immun. 65*, 150−155.
6. Sikkema, D. J., and Murphy, T. F. (1992) Molecular analysis of the P2 porin protein of nontypeable *Haemophilus influenzae*, *Infect. Immun. 60*, 5204−5211.
7. Bell, J., Grass, S., Jeanteur, D., and Munson, R. S., Jr. (1994) Diversity of the P2 protein among nontypeable *Haemophilus influenzae* isolates, *Infect. Immun. 62*, 2639−2643.
8. Galdiero, S., Capasso, D., Vitiello, M., D'Isanto, M., Pedone, C., and Galdiero, M. (2003) Role of surface-exposed loops of *Haemophilus influenzae* protein P2 in the mitogen-activated protein kinase cascade, *Infect. Immun. 71*, 2798−2809.
9. Srikumar, R., Dahan, D., Gras, M. F., Ratcliffe, M. J., van Alphen, L., and Coulton, J. W. (1992) Antigenic sites on porin of *Haemophilus influenzae* type b: mapping with synthetic peptides and evaluation of structure predictions, *J. Bacteriol. 174*, 4007−4016.
10. Saint, N., Lou, K. L., Widmer, C., Luckey, M., Schirmer, T., and Rosenbusch, J. P. (1996) Structural and functional characterization of OmpF porin mutants selected for larger pore size. II. Functional characterization, *J. Biol. Chem. 271*, 20676−20680.
11. Dinarello, C. A. (1991) The proinflammatory cytokines interleukin-1 and tumor necrosis factor and treatment of the septic shock syndrome, *J. Infect. Dis. 163*, 1177−1184.
12. Van Snick, J. (1990) Interleukin-6: an overview, *Annu. Rev. Immunol. 8*, 253−278.
13. Van Amersfoort, E. S., Van Berkel, T. J., and Kuiper, J. (2003) Receptors, mediators, and mechanisms involved in bacterial sepsis and septic shock, *Clin. Microbiol. Rev. 16*, 379−414.
14. Galdiero, M., Tortora, A., Damiano, N., Vitiello, M., Longanella, A., and Galdiero, E. (2005) Induction of cytokine mRNA expression in U937 cells by *Salmonella typhimurium* porins is regulated by different phosphorylation pathways, *Med. Microbiol. Immunol. 194*, 13−23.
15. Rawadi, G., and Dussurget, O. (1995) Advances in PCR-based detection of mycoplasmas contaminating cell cultures, *PCR Methods Appl. 4*, 199−208.
16. Coulton, J. W., and Wan, I. F. (1983) The outer membrane of *Haemophilus influenzae* type b: cell envelope associations of major proteins, *Can. J. Microbiol. 29*, 280−287.
17. Galdiero, M., D'Amico, M., Gorga, F., Di Filippo, C., D'Isanto, M., Vitiello, M., Longanella, A., and Tortora, A. (2001) *Haemophilus influenzae* porin contributes to signaling of the inflammatory cascade in rat brain, *Infect. Immun. 69*, 221−227.
18. Lowry, O. H., Rosebrough, N. J., Farr, A. L., and Randall, R. J. (1951) Protein measurement with the Folin phenol reagent, *J. Biol. Chem. 193*, 265−275.
19. Laemmli, U. K. (1970). Cleavage of structural proteins during the assembly of the head of bacteriophage T4, *Nature* 277, 680−685.
20. Tsai, C. M., and Frasch, C. E. (1982) A sensitive silver stain for detecting lipopolysaccharides in polyacrylamide gels, *Anal. Biochem. 119*, 115−119.
21. Yin, E. T., Galanos, C., Kinsky, S., Bradshaw, R. A., Wessler, S., Luderity, O., and Sarmiento, M. F. (1972) Picogram-sensitive assay for endotoxin: gelation of *Limulus polyphemus* blood cell lysate induced by purified lipopolysaccharides and lipid A from Gram-negative bacteria, *Biochim. Biophys. Acta 261*, 284−289.
22. Nikaido, H., and Rosenberg, E. Y. (1983) Porin channels in *Escherichia coli*: studies with liposomes reconstituted from purified proteins, *J. Bacteriol.* 153, 241−252.
23. Bonny, C., Oberson, A., Negri, S., Sauser, C., and Schorderet, D. F. (2001) Cell-permeable peptide inhibitors of JNK: novel blockers of beta-cell death, *Diabetes 50*, 77−82.
24. Cuenda, A., Rouse, J., Doza, Y. N., Meier, R., Cohen, P., Gallagher, T. F., Yang, P. R., and Lee, J. C. (1995) SB 203580 is a specific inhibitor of a MAP kinase homologue which is stimulated by cellular stresses and interleukin-1, *FEBS Lett. 364*, 229−233.
25. Singh, J., Chuaqui, C. E., Boriack-Sjodin, P. A., Lee, W. C., Pontz, T., Corbley, M. J., Cheung, H. K., Arduini, R. M., Mead, J. N., Newman, M. N., Papadatos, J. L., Bowes, S., Josiah, S., and Ling, L. E. (2003) Successful shape-based virtual screening: the discovery of a potent inhibitor of the type I TGFbeta receptor kinase (TbetaRI), *Bioorg. Med. Chem. Lett.13*, 4355−4359.
26. Chakrabartty, A., Kortemme, T., and Baldwin, R. L. (1994) Helix propensities of the amino acids measured in alanine-based peptides without helix-stabilizing side-chain interactions, *Protein Sci. 3*, 843−852.
27. Simmerling, C. L., Darden, T. A., Merz, K. M., Stanton, R. V., Cheng, A. L., Vincent, J. J., Crowley, M., Tsui, V., Radmer, R., Duan, Y., et al. (1999) AMBER 6, University of California, San Francisco, CA.
28. Koradi, R., Billeter, M., and Wüthrich, K. (1996) MOLMOL: a program for display and analysis of macromolecular structures, *J. Mol. Graphics 14*, 51−55.
29. Altschul, S. F., Madden, T. L., Schäffer, A. A., Zhang, J., Zhang, Z., Miller, W., and Lipman, D. J. (1997) Gapped BLAST and PSI-BLAST: a new generation of protein database search programs, *Nucleic Acids Res. 25*, 3389−3402.
30. Cornell, W. D., Cieplak, P., Bayly, C. I., Gould, I. R., Merz, K. M., Jr., Ferguson, D. M., Spellmeyer, D. C., Fox, T., Caldwell, J. W., and Kollman, P. A. (1995) A second generation force field for the simulation of proteins, nucleic acids, and organic molecules, *J. Am. Chem. Soc. 117*, 5179−5197.
31. Saviano, G., Benedetti, E., Cozzolino, R., De Capua, A., Laccetti, P., Palladino, P., Zanotti, G., Amodeo, P., Tancredi, T., and Rossi, F. (2004) Influence of conformational flexibility on biological activity in cyclic astin analogues, *Biopolymers 76*, 477−484.
32. Jorgensen, W. L., Chandrasekhar, J., Madura, J., and Klein, M. L. (1983) Comparison of simple potential functions for simulating liquid water, *J. Chem. Phys. 79*, 926−935.
33. Vitale, R. M., Zaccaro, L., Di Blasio, B., Fattorusso, R., Isernia, C., Amodeo, P., Pedone, C., and Saviano, M. (2003) Conformational features of human melanin-concentrating hormone: an NMR and computational analysis, *ChemBioChem 4*, 73−81.
34. Berman, H. M., Westbrook, J., Feng, Z., Gilliland, G., Bhat, T. N., Weissig, H., Shindyalov, I. N., and Bourne, P. E. (2000) The protein data bank, *Nucleic Acids Res. 28*, 235−242.
35. Hutchinson, E. G., and Thornton, J. M. (1994) A revised set of potentials for beta-turn formation in proteins, *Protein Sci. 3*, 2207−2216.

36. Abad-Zapatero, C., Goldman, R., Muchmore, S. W., Hutchins, C., Stewart, K., Navaza, J., Payne, C. D., and Ray, T. L. (1996) Structure of a secreted aspartic protease from *C. albicans* complexed with a potent inhibitor: implications for the design of antifungal agents, *Protein Sci. 5*, 640−652.
37. Li, S., Kelly, S. J., Lamani, E., Ferraroni, M., and Jedrzejas, M. J. (2000) Structural basis of hyaluronan degradation by *Streptococcus pneumoniae* hyaluronate lyase, *EMBO J. 19*,1228−1240.
38. Singh, S. K., Matsuno, K., LaPorte, D. C., and Banaszak, L. J. (2001) Crystal structure of *Bacillus subtilis* isocitrate dehydrogenase at 1.55 Å. Insights into the nature of substrate specificity exhibited by *Escherichia coli* isocitrate dehydrogenase kinase/phosphatase, *J. Biol. Chem. 276*, 26154−26163.
39. Muller, D. J., and Engel, A. (1999) Voltage and pH-induced channel closure of porin OmpF visualized by atomic force microscopy, *J. Mol. Biol. 285*, 1347−1351.
40. Massari, P., Ram, S., Macleod, H., and Wetzler, L. M. (2003) The role of porins in neisserial pathogenesis and immunity, *Trends Microbiol. 11*, 87−93.

BI052262P